Instrumented indentation of an elastomeric material, protocol and application to vulcanization gradient

Clémence Fradet, Florian Lacroix, Gaelle Berton, Stéphane Méo, Eric Le Bourhis

Version of Record: https://www.sciencedirect.com/science/article/pii/S0142941819307652
Manuscript_3c9db52c3f2d4dd2f6134a2d1f18ff87

Instrumented indentation of an elastomeric material, protocol and application to vulcanization gradient

Authors

Clémence Fradet[1], Florian Lacroix[1], Gaëlle Berton[1], Stéphane Méo[1] and Eric Le Bourhis[2]

Affiliations

[1] Laboratoire de Mécanique Gabriel Lamé, Université de Tours, Université d'Orléans, INSA Centre Val de Loire, Polytech Tours, 7 avenue Marcel Dassault BP40, 37004 Tours, France

[2] Institut P', CNRS-Université de Poitiers-ENSMA-UPR3346, SP2MI-Téléport, 2 boulevard Marie et Pierre Curie, BP30179, 86962 Futuroscope-Chasseneuil Cedex, France

Corresponding author

Clémence Fradet

Email addresses

clemence.fradet@univ-tours.fr

florian.lacroix@univ-tours.fr

gaelle.berton@univ-tours.fr

stephane.meo@univ-tours.fr

eric.le.bourhis@univ-poitiers.fr

Abstract

Instrumented Indentation Testing is applied on a fluoroelastomer so as to get information about the local mechanical response of such a rubbery material. Due to their viscoelasticity, elastomers exhibit a time-dependence, responsible for a variation in their behavior as a function of the stress or strain rate. A few studies highlight modifications of the indentation hardness H and modulus E_r when the load function varies. However, these works concern polymers and, to our knowledge, such an investigation has not yet been carried out on elastomeric materials. Results about the influence of the loading-unloading procedure on E_r are presented here. They show elastic modulus' variations depending on the chosen protocol's time scale and reported evolutions are consistent with the expected behavior of viscoelastic materials. Furthermore, in preparation of this main study, preliminary verifications were necessary since sources of error are known to distort indentation results. A focus on the microstructure and roughness is presented in this paper and reveals, in particular, a non-negligible improvement of indentation curves (load-displacement hystereses) with an appropriate sample preparation and surface finish. These results have finally been used as a basis for the study of local gradients within a rubber sample. This study revealed a gradient (i.e. an increasing modulus) from the outer part of the sample to the inner one, attributed to thermal effects during the molding.

Keywords

Indentation, elastomer, protocol, gradient

1. Introduction

Instrumented indentation testing (IIT) is recognized as a very powerful measurement method thanks to decades of theoretical developments and improvement of instruments' sensitivity and automation. In various materials' science fields, empirical observations as well as modelling allowed the IIT's growth through deeper understandings of local mechanisms. Indeed, IIT is no more restricted to metals as it was at the very beginning of the development of hardness tests in the early of the 20th century [1,2]. One can find in the literature many uses of it: from industrial to medical applications through more fundamental researches. All types of behaviors and structures are represented in IIT's literature: from very hard to very soft materials ; elastic, plastic and/or viscoelastic behaviors ; adhesive, but also coatings, composites, biological tissues.

However, some of these characteristics and behaviors make a number of materials challenging to indent in terms of experimental set up as well as data analyses. Elastomers are one of these. Locally, elastomers are defined by a structure made of macromolecular chains with a carbon or silicon backbone [3]. Without any other transformation, the material is a raw rubber gum, which does not possess any interesting mechanical properties. The final elastomeric properties can only be obtained after the main chains' crosslinking. The curing process (involving the vulcanization *i.e.* the crosslinking process) consists in a chemical reaction between a curing agent, typically sulfur or peroxide, and the

macromolecular chains of rubber, activated at high temperature. Latter operation allows the creation of a three-dimensional complex network with non-linear elasticity at high deformations [4–7] and time-dependent response [6,8,9].

Performances of rubber mixes can also be adjusted with additives. One can cite reinforcement fillers, like carbon black or silica, which are one of the most important components of elastomers mixtures. They are made of particles organized in aggregates [10,11], which are the smallest indivisible units of fillers. Then, the merging of several aggregates constitutes much bigger agglomerates whose dimensions can reach a few tens of microns. The addition of them in the rubber gum leads to a secondary network in the material and thus better properties [12–14] but is also responsible for local heterogeneities [15].

IIT is adapted to probe the heterogeneous nature of such materials. Great theoretical advances have been made since the contact mechanics by Hertz [16,17] and Boussinesq [18] at the end of the 19th century, the important contributions of Love [19] and Sneddon [20], to the internationally used method of Oliver and Pharr [21,22]. However, common assumptions are found in all these works *i.e.* a semi-infinite and homogeneous space, an infinitely rigid indenter (except for Hertz), a purely elastic behavior of the sample and a smooth and frictionless contact. A large amount of work has been expended to extend this framework to a large range of materials [23]. Let us notice that, mainly due to their viscoelasticity and high compliance resulting in relatively large displacements for small forces, indenting rubbers is very challenging. Moreover both heterogeneity and roughness of samples harden the analysis.

Historically, theoretical developments and experiments of IIT concern homogeneous and isotropic materials. However, many materials are composites ones at a given scale according to the presence of ingredients, grains or fillers embedded in a matrix. Among these multiscale or multiphase materials one can cite cement-based materials [24], metals [25] and bone [26], which can be treated as homogeneous at the macroscopic level (larger than the cm length scale) but must be considered as heterogeneous at a finer level of observation (from the nm to the cm length scale). The heterogeneity may cause difficulties since the continuum indentation analysis assumes the stress-strain relationship and the indentation hardness H independent on the length scale (defined by the indentation depth h for example) [24]. For heterogeneous materials, it is easily understandable that indentation curves and results may change and exhibit a lack of reproducibility as a function of the indentation location, and as a function of the tip/sample contact in comparison with the representative volume element (RVE). To avoid any microstructural effects and get homogenized mechanical properties (rather than the individual responses of each phases), tests should be carried out so as to reach an indentation depth h much larger than the characteristic size of the inclusions D (*i.e.* $h \gg D$, or more specifically $h > 6D$ [27]). Fillers' agglomerates described above constitute heterogeneities at the micrometer scale. Thus, relatively large indentation dimensions should be used and will be easily achievable with the high compliance of such materials.

Another factor known to be responsible for experimental errors in small scale instrumented indentation is the roughness of samples. Issues on both the indentation hardness H and the elastic modulus E_r during the nanoindentation of rough surfaces have been studied by a few teams. Its impact on these measurements is studied from different points of view thanks to experiments and also numerical simulations leading to model developments [28]. In terms of results, it has been

observed for example that the roughness causes adhesion issues during Atomic Force Microscopy (AFM) tests [29], and overestimations of the measured values of H and E_r in nanoindentation. In other words the roughness of indented surface could be one of the explanations of the so-called Indentation Size Effect [30]. Moreover, analyses difficulties are induced by the important scatter in measurements [31], which is the direct consequence of the contact's topography. The topography is described by the shape of the asperities of the sample, their spatial distribution and density and also by the distribution of their heights and widths [23,32]. Finally, this issue is treated in the ISO Standard 14577 which specifies that the arithmetic roughness R_a does not generate measurement uncertainties as long as it is less than 5% of the indentation contact depth. This condition can be easily obtained on materials like metals, on which a mirror finish polishing can be carried out. However, as a result of their high compliance, polishing is not realistically feasible on elastomeric materials and could lead to alteration of properties, even damages by friction, self-heating or residual stresses. Regarding all these limitations, reaching a low roughness on elastomers appears to be an important technical and scientific challenge.

Since 2000, IIT has been used on rubber-like materials [33–35]. Nevertheless, to our knowledge, a large part of published works are related to indentation carried out on silicones, often PDMS (PolyDiMethyl Siloxane) [36–41] which are far from representing the great diversity of elastomeric materials. In addition, characterized rubbers are often unfilled and much more elastic than viscoelastic which makes them materials far from real used ones and makes them easier to study.

In this work, a filled fluoroelastomer (material used in the aviation industry) was employed to apprehend the accuracy of the use of IIT on rubber-like materials. In a first step, characterizations under different protocols were carried out so as to ensure a satisfactory sample's quality and to set a load function whose kinematics allows to avoid severe viscoelastic effects. Some observations and results will be correlated to global tests. Then, these investigations made possible the study of a well-known, but rarely observed, phenomenon: local gradients within samples after curing. This study allowed both the acquisition of precious information about the importance of the curing process to get performant elastomer products, and the demonstration of all the potential of IIT as a local probe and mapping tool.

2. Material

The studied rubber blend [42] is extensively used in industrial elastomer's tubes for harnesses' protection in an aeronautical application. Its gum base is a fluoroelastomer (FKM) *i.e.* a special rubber designed to withstand severe chemical and thermal conditions. The following experimental characterizations involve peroxide vulcanizates, reinforced by carbon black and silica. The raw rubber blend was elaborated by introducing all the ingredients into an internal mixer and was then pressed and cured so as to get 2-millimeters-thick sheets. The curing process was carried out for 20 min at 180°C within the mold of the press and was followed by a post-curing step realized in an oven for 2 h at 200°C. Samples were finally extracted from the 2-mm-thick sheets.

3. Methods

This section presents the main technique of the study (IIT) as well as other instruments required for preliminary verifications and complementary tests.

3.1. White light interferometry

An optical equipment Wyko NT1100 using white light interferometry was used to appreciate the quality of the surfaces to be tested in terms of roughness. Two types of surfaces were characterized: the external surface of the sheet *i.e.* the surface in contact with the mold during the molding step and cross-sectional slices cut with new (unused) razor blades. The molded surface appears matt and possesses a non-negligible roughness while the prepared cross-sections are reflective and appear smoother. A surface preparation with a cryo-microtome had also been tested, however this technique resulted in a surface with several cutter scratch traces and so an unsatisfying surface finish. Hence, this preparation technique has not been used. For each type of surfaces, measurements were repeated at least ten times at different and randomly chosen areas.

3.2. Transmission Electron Microscopy

Microstructural observations were made on a JEOL 1230 120kV Transmission Electron Microscope. Samples were preliminary cryo-ultramicrotomed at -40 °C, using a diamond knife, on a Leica Ultracut UCT. The obtained 100-nm-thick samples were finally transferred onto a Cu+C mesh grid to be observed.

3.3. Instrumented Indentation Testing (IIT)

Indentation tests have been performed using a Bruker's Hysitron TI 980 TriboIndenter with the high resolution nanoDMA head allowing forces and displacements up to 10 mN and 15 µm respectively, on which a diamond Berkovich tip was mounted. To limit measurements artifacts linked to the surface quality, it has been decided to carry out indentation tests on cross-sections prepared with razor blades. Samples were glued on a support which was itself maintained on the machine by vacuum. All tests were made with the force controlled quasi-static mode applying a trapezoidal load function. A maximal force P_{max} of 1 mN has been chosen. Indeed, it turns out that, on the currently studied material, this load is small enough to extract the local mechanical response and large enough to limit scatter and previously cited error sources. The load function has been varied by applying a wide range of loading kinematics:

(i) Variation of the loading time $t_L = \{2, 10, 50, 100, 300, 1000\}$ s, with fixed holding and unloading times, respectively 300 s and 100 s

(ii) Variation of the holding time $t_H = \{10, 60, 100, 300, 1800\}$ s, with 100 s of loading and unloading times

(iii) Variation of the unloading time $t_U = \{2, 5, 10, 50, 100, 1000\}$ s, with 100 s of loading and 300 s of holding time

Each test was repeated at least eight times so as to get averaged values on at least five measurements after removal of failed tests and abnormal curves.

Finally, it has been decided to analyze the experimental hystereses with Oliver and Pharr method using Eqs. 1 to 4 [21,22]. According to them and to the ISO Standard 14577, unloading curves were fitted from 100% to 20% of P_{max}.

Indentation curves were analyzed as follows. The upper part of the unloading curve can be mathematically described by the power law function:

$$\boldsymbol{P = A\left(h - h_f\right)^m} \quad (1)$$

With $\boldsymbol{P}$ and $\boldsymbol{h}$ the measured force and displacement respectively. $\boldsymbol{A}$, $\boldsymbol{h_f}$ and $\boldsymbol{m}$ are fitting coefficients estimated by the least square method.

The derivation of this equation allows to obtain the contact stiffness between the indenter and the material, $S = dP/dh_{|h=h_{max}}$ while the contact depth h_c is determined as:

$$\boldsymbol{h_c = h_{max} - \varepsilon \frac{P_{max}}{S}} \quad (2)$$

With $\boldsymbol{P_{max}}$ and $\boldsymbol{h_{max}}$ the maximal force and displacement respectively and $\boldsymbol{\varepsilon}$ a correction factor equal to 0.75 for a Berkovich tip [21].

At this given depth, the projected contact area A_p between the indentation tip and the sample is:

$$A_p = 24.5\ {h_c}^2 \quad (3)$$

It has been decided to use this perfect projected contact area because, for currently used indentation depths, the apex default can be considered as negligible.

Finally, the indentation modulus was obtained as:

$$E_r = \frac{S\sqrt{\pi}}{2\beta\sqrt{A_p}} \quad (4)$$

With β, a coefficient equals to 1.034 for a Berkovich indenter [22].

3.4. Macroscopic tensile and creep tests

Macroscopic tensile and creep tests were made on standard H2 dumbbell samples (ISO 37) using a Zwick Z010 tensile machine on which a 10 kN load cell was mounted. Tests consisted in: a stretching phase up to 40 N with four different tensile loading rates ranged from 20 $N.s^{-1}$ to 0.04 $N.s^{-1}$. The target force was then held constant during 300 s. Resulting stress and strain undergone by the material were around 4.5 MPa and 160% respectively. Each test was repeated three times and results were averaged.

4. Results and Discussion

This section presents the results obtained from indentation testing. Before proceeding to these tests, the influence, or more specifically the absence of influence, of the sample's roughness and microstructure has been checked. Then, discussions on how the indentation provides information about the local behavior of rubbers are made.

4.1. Elastomer surfaces and structure

4.1.1. Roughness

The morphology of samples has been studied from the point of view of the indented surface quality by quantifying the arithmetic roughness R_a. Observations of the surface finishes for the two differently prepared types (molded or cut) are shown in Figure 1. The indentation projection at maximum load is schematically represented in the lower-left corner insets. It can be easily noticed that the molded surface presents asperities with lateral length scale of 50-100 µm while the measured roughness is $R_a = 547 \pm 106$ nm (Fig. 1a). The typical size of the projected contact area which is about 50 µm at maximum load is of the same magnitude as asperities. Hence, with our contact depth h_c around 5700 nm, the recommendation of the ISO standard is unreachable because of the poor surface quality obtained after molding. Under this condition, it seems obvious that indentation results will be affected by their relative location compared to the surface's reliefs. However, the roughness has been significantly improved with the razor blade cutting. Indeed, the roughness after this preparation is $R_a = 100 \pm 32$ nm (Fig. 1b). This represents an average roughness five times less than that of the molded surface. An improvement is also observed in terms of dispersion (standard deviation), although, its relative value remains high. So far, it is the absolute roughness that rules the indentation dispersion as discussed in more details below. Optical surfaces' controls were completed by indentation tests so as to understand how the roughness really impacts the reproducibility of them. As shown on Figure 2, the first impact of the roughness when considering indentation results is a loss of the hystereses' quality between a smooth and a rough surface: curves acquired on the rough (molded, Fig. 2a) one are noisy while those obtained on the smooth (cut, Fig. 2b) one are not. Also, a large dispersion of the loading-unloading curves is observed in the case of a molded surface with residual penetration difference of 800 nm, while this difference decreases to about 40 nm in the case of a cut cross sectional slice. Indeed, on a molded sample, when the load increases, the tip first comes into contact with the highest hills and then conforms to the surface progressively. Thus, the contact is not continuous but is made in successive tiny increments, which is visible on indentation curves. Figure 2 also clearly indicates an important lack of reproducibility of indentation curves when testing the molded surface while hystereses obtained on the prepared surface overlap almost perfectly on cut surfaces. From the point of view of E_r, the resulting standard deviations represent 11% of the mean value for the rough surface and only 2% for the prepared one. Consequently, with such an improvement in reproducibility, material's phenomena should not be hidden by the measurements scatters and the extraction of relevant trends in the following section was feasible.

FIGURE 1

FIGURE 2

4.1.2. Microstructure

T.E.M. micrographs allowed to study the local composition of the studied material and revealed the different material's phases, particularly carbon black inclusions in the elastomer matrix. The comparison between the length scale of these local heterogeneities and the typical dimensions of an indent made at 1 mN is presented in Figure 3. On this micrograph, one can see the microcomposite nature of the fluoroelastomer as shown by the presence of different phases homogeneously distributed: the rubber matrix (light grey), small and well-dispersed carbon black agglomerates (black) and very tiny silica agglomerates (intermediate grey). White spots are voids in the sample. Silica and carbon black clearly compose a secondary network. However, despite this complex microstructure, the contact region is large enough to consider the material as homogeneous and so to avoid any scatter in measurements regarding the indented location. Consequently, indentation results of this study will be considered as independent of the microstructure and the response of the material will be treated as an averaged one, as in the case of bulk tests.

FIGURE 3

It is worth reminding that the microstructure and roughness being scale-related issues, previous conclusions are only consistent in the case of indents reaching displacements larger than or equal to currently presented ones.

4.2. Effect of loading-unloading procedure

Due to their time dependence, rubbers are known to be very sensitive to loading or displacement rates employed in characterization methods.

The study of the effect of the loading-unloading procedure on indentation results has been made regarding the indentation reduced modulus E_r. This parameter has been chosen for its consistence and its common use in instrumented indentation. However, being dependent on the popular model proposed by Oliver and Pharr [21,22] and on the fitting procedure, in particular the fitted portion of the upper part of the unloading curve, it has been decided to analyze the results in terms of other quantities which are the displacements. The advantage of displacements is that they can be considered as raw data since they are the result of a direct instrument's measurement and are therefore independent from the applied analysis method and the theory behind it.

4.2.1. Loading rate influence

Figure 4 shows averaged loading curves as a function of the applied loading rate. Its influence is easily noticeable. As expected, a fast penetration velocity leads to a lower displacement of the tip. This behavior is characteristic of the viscoelastic nature of the elastomer. Indeed, in such a material, the resistance of the microstructure, in particular the macromolecular chains, is dependent on the way it is stressed. From this observation it can be concluded that it does not exist a unique response of an elastomer to the loading rate so that the obtained behavior is not intrinsic but deeply linked to the chosen experimental conditions. To further examine the impact of the loading rate, all the displacements of the different loading phases have been analyzed. Figure 5 presents the displacements at the end of the loading stage (h_L), during the holding stage (h_H) and also the sum of

them *i.e.* the maximal depth h_{max}. The decrease of h_L with the increase of the loading rate observed in Figure 4 is confirmed here. It can also be noticed that the displacement during the holding step h_H increases in the same trend so that the maximal depth is unchanged whatever the loading rate. In other words, the displacements during the loading and the creeping stages balance one another.

Also, creep curves presented in Figure 6 reveal a strong influence of the loading rate on the strain mechanisms under a constant load. Two stages are observed on these curves, namely the primary and secondary creep. The first one, also called transient creep, occurs on the early part of curves and is characterized by a sharp increase of the creep depth and thus a non-constant strain rate. Just after a fast loading phase, the material is in such a state of viscoelastic deformation that the primary creep is very important. This primary creep is followed by a steady state, described by a nearly stable rise in creep depth *i.e.* a constant value of the displacement rate. On Figure 6, one can see that this secondary creep also changes with the loading time. Indeed, the stabilized displacement rate decreases with increasing loading times. These observations are consistent with those made on viscoelastic materials [43,44]. Finally, even though the loading rate does not appear to influence the behavior of the elastomer after the two first steps of loading and holding (regarding the equilibrium of their displacements), the unloading curve seems to be sensitive to it. Indeed, with an increasing loading rate (the holding stage remaining constant), the unloading recovery increases leading to a decreasing unloading stiffness S. According to Eq. 4, this evolution of S, combined with a decreasing contact depth h_c and thus of the projected contact area A_p, can explain a slightly decreasing E_r (Figure 7). However, considering almost three decades of tested loading kinematics, this decrease could be considered as negligible and so E_r seems to be quasi-independent from this experimental parameter. In the literature, E_r is shown to exhibit evolution rates much higher. On polymers, Fu et al. [43] for example found moduli values 10% higher between fast and slow loadings, by testing different rates in a range of one decade: 5.35 GPa at 6 mN/s and 4.8 GPa at 0.25 mN/s. Also Jin et al. [45] found an evolution rate of 250% on two decades: 4.5 GPa at 3 mN/s and 1.3 GPa at 0.0375 mN/s. Hence, the indentation moduli of polymers seem to be much more sensitive to the loading rate in comparison to elastomers.

FIGURE 4

FIGURE 5

FIGURE 6

FIGURE 7

4.2.2. Holding time influence

The time dependence of the studied rubber was also examined under various holding times at the maximal force. When this force is held constant, the tip continues to sink into the surface because of the elastomer's viscoelastic response, as a classic creep test. Figure 8 shows the induced creep displacement as a function of the duration of the holding segment t_H. As expected, the total displacement during the holding stage continuously grows with its duration. In the literature, it is recommended to use large holding times to remove viscoelastic effects as much as possible [45] and thus to approach the conditions of use of the model of Oliver and Pharr. However, such a recommendation can lead to excessive experimental times so that on very viscoelastic materials a

purely elastic behavior during the unloading, *i.e.* just after the holding period, is almost unreachable. The observed increase in the holding displacement is responsible for an increasing total depth h_{max} and consequently A_p, which is 1.5 times higher after 1800 s than after 10 s. The increase in displacements naturally leads to lower elastic moduli according to Eqs. 3 and 4. Under this condition, the apparent reduced modulus E_r is affected by this experimental stage since it loses about 10% of its value when a long t_H is used (Figure 9). This modulus softening has also been observed in the literature, on polymers like PMMA [45] or epoxy [46].

FIGURE 8

FIGURE 9

4.2.3. Unloading rate influence

FKM exhibits a strong dependence on the unloading rate, further illustrating its viscoelastic behavior. This parameter is essential since the theory is based upon the mathematical analysis of the unloading curve, which is assumed to be purely elastic. On Figures 10 and 11, one can observe a noticeable difference of the recovery behavior of the material between fast and slow rates. Indeed, when the tip is removed in a short period of time, the material exhibits a stiff and highly viscoelastic response as shown by the low values of the unloading displacement h_U (defined as $h_U = h_{max} - h_{final}$, with h_{final} the displacement at the end of the unloading *i.e.* at zero force) while a slow mechanical solicitation allows the observation of its elastic deformation. With slow rates, an important recovery is observed, leading automatically to low values of the contact stiffness S. Thus, decreasing elastic moduli E_r were observed when a slower unloading rate was chosen (Figure 12). This behavior is expected considering the viscoelastic nature of the studied material but is not in accordance with literature results. Indeed, through experimental observations made on polymers [45,47], it is generally accepted that low unloading velocities causes high values of E_r, or in the most severe conditions, a “nose effect” may appear in the upper part of the unloading curve. In the present case, an opposite trend is observed since the highest moduli are obtained for fast unloading ones and in fact the “nose effect” was never observed even with an unloading rate as low as $-0.001\ mN/s$. One reason for that is the long holding period prior to the unloading stage. Indeed, the material was allowed to creep for 300 s, a time long enough to limit viscoelastic effects upon unloading. An elastomer is also more compliant than a polymer with a relative limited viscoelastic response in the elastomeric plateau.

FIGURE 10

FIGURE 11

FIGURE 12

To conclude on this part, through the study of the loading-holding-unloading procedure, the importance of the viscoelastic response of the elastomer tested by IIT has been apprehended. Moreover, regarding this viscoelasticity, all the observed behaviors are consistent with the expected ones *e.g.* stiff responses for high rates and compliant ones for low velocities. Also, due to the viscosity of the FKM, it has been noticed a non-negligible impact of the mechanical history on its response *i.e.* the kinematic of the loading phase will directly impact the strain mechanisms of the

following ones. As a consequence, an intrinsic modulus of this type of material cannot be obtained since, whatever the protocol, the viscosity effect cannot be entirely removed. This leads to a non-unicity of the modulus since it is a combination of both the elastic and viscous nature of the rubber but with different ratios between the elasticity and the viscosity as a function of the solicitation. In other words, on elastomers, there are no under- or overestimated modulus' values but a given mechanical response (more or less stiff or compliant) corresponding to a particular solicitation. IIT could therefore be used to appreciate the viscoelasticity of rubbers.

Finally, for the rest of the study, the following parameters have been chosen: $\pm 0.01\ mN/s$ for the loading and unloading stages and 300 s of holding time. According to previous discussions this protocol is not the only one that could have been taken, so the choice was made to balance both time constraints and viscoelastic effects (*e.g.* the "nose effect").

4.2.4. Comparison with global tests

Experiments exploring the influence of the loading rate have been carried out at the global scale. Data extraction concerned the displacements: the displacement reached during the stretching step, the one reached under holding and the sum of them *i.e*. the total displacement. Typical curves are given in Figure 13. Figure 14 summarizes the results. In both tests (IIT and macroscopic tensile tests), a very satisfactory reproducibility of measurements has been noticed: the coefficient of variation (ratio between the standard deviation and the mean value, in percentage) does not exceed 6.5% for the first one and 1.5% for the second one. The value of this coefficient is much better in the case of global tests because of the higher sensitivity of IIT to environmental, instrumental and material factors, leading to more scattered results. Furthermore, similarly to the observed behavior in IIT, it can be seen that the total displacement is independent of the loading rate. Indeed, with a fast loading rate the high mechanical stress cannot be accommodated by the material, so that the strain during this step remains limited. As a consequence, the missing strain will be recovered during the holding period through the transient creep. Also, the comparison of the local (Figure 5) and global (Figure 14) tests seems to reveal analogous trends, indicating similar mechanisms involved at these two scales. Finally, the holding to total displacement ratio, $h_H/h_{max} \times 100$, has been quantified. For the two types of tests, this ratio gives the same value with a 1000-s-loading time *i.e*. 5% of the total displacement is due to creep, while the other 95% were obtained during the loading. Differences between macro- and microscopic results appear with shorter loading times. This may be due to the impact of the viscosity, which might not be necessarily the same when testing the global and the local scales. Also, the comparison between local and global measurements must be made with caution since stress and strain conditions are quite different, and global tests consisted in uniaxial tension while indentation imposes a triaxial compression solicitation.

FIGURE 13

FIGURE 14

4.3. Application to properties gradients

Rubbers are materials which have been cured, in a mold and under press in the case of laboratory sheets. Consequently, the heating source being external, one can expect an inner part less cured than the outer one, especially if the curing time is not sufficient to allow the diffusion of the heat inside the material. Thus, it is generally supposed that the skin of rubber parts is stiffer than the bulk [48,49] if such a difference in curing process occurs. In this section, the main aim was to probe the FKM mechanical properties and monitor changes along the thickness of the specimens.

Indentation profiles were performed in cross-sectional slices of FKM cut with razor blade. A typical profile consists in a linear pattern made of 20 successive indents. The first indent was carried out at 20 µm from the edge of the sample, and then each indent was performed at 50 µm from the previous one so as to get a 1-mm-long profile. Indeed, to reduce experimental times, it has been decided to characterize only half of the thickness of the rubber sheet (1 mm instead of 2 mm) with the assumption that mechanical properties inside it are symmetric. This assumption was examined through few tests, which seemed to reveal no differences in profiles, whatever the departure edge (Fig. 15). For each sample to characterize, 4 to 6 profiles were carried out.

FIGURE 15

Figure 16 shows the averaged evolution of the indentation modulus in the thickness of the sample. One can notice the increasing type of the gradient. Several variations were detected. More precisely, near the edge, moduli are low and progressively increase. This increase occurs up to 500 µm, distance at which the modulus reaches a peak. Then, between 500 and 1000 µm, the modulus loses part of its value.

The first assumption to explain low moduli values at the beginning of the profile is the vicinity of the edge. Indeed, when an indent is performed near an edge, the applied force could cause the deflection of this edge due to an insufficient resistance of the sample (in comparison with an indent made in the bulk [50,51]). The direct consequence of this is an increase of the displacements, responsible for lower mechanical properties. However, such an edge effect is expected to occur at the very close vicinity of the edge while E_r continuously increases up to 400 microns *i.e*. quite far from the edge. Additional answers are provided by the Figure 17, on which the maximal displacement h_{max} is studied. One can notice that it is actually higher near the edge. However, its value stabilizes faster than E_r: it decreases within approximately 300 µm and then reaches a constant value. Thus, the measurement artifact induced by the presence of the edge has to be ruled out. It revealed a change of the material's properties. Finally, tests performed in the middle of the rubber sheet (around 1000 µm) seem to reveal a decreasing indentation modulus correlated with an increasing total displacement. This may indicate a different state of vulcanization: the material being less cured (*i.e.* less stiff) when the center of the sample is approached.

In elastomeric materials, the widely accepted idea in terms of gradient is that there is a core less cured, and thus softer, than the skin. This is detected here, however a softening of the extreme skin is also observed. As a reminder, according to the heat propagation into the material and the associated curing rate, one could find higher moduli near the edge and then a decrease of it. Such observations on elastomers can be found in literature [48,49]. Let us notice that the reference [48] also shows a no-evolution of the moduli as a function of the measurement position within the thickness of rubber samples (700 µm thick). Authors observed either results when the elastomer's chemical formula was changed. Similar trends to currently presented ones were observed on

injection molded HDPE polymers [52,53]: higher moduli in the core region than for the skin and trans-crystalline layers. In paper [52], this gradient is attributed to the phase morphology formed during the injection process: a trans-crystalline region exhibits higher moduli than an amorphous one. Also, in [53], various other gradients' shapes can be found on another HDPE and POM: local profiles are complex and wavy, due to several trans-crystalline and intermediate zones. These studies clearly show the great diversity of the shape of local gradients.

Finally, in present case, local measurements allow the observation of important gradients within a sample. Indeed, Figure 16 reveals a modulus' amplitude of 12 MPa (20 MPa for higher values and 8 MPa for lower ones). More global tests would have given more averaged values, which would hide the fine trends shown by local ones.

FIGURE 16

FIGURE 17

5. Conclusions

In this paper, Instrumented Indentation Testing carried out on a FKM elastomer was presented. The main aim of the study was to probe the local mechanical properties of this elastomer and capture possible gradients. An upstream work was necessary to measure the impact of the experimental procedure on results so as to develop a robust methodology, whose results can be trusted.

In a first step, preliminary checks allowed to ensure that the microstructure and roughness were not responsible for bias in results. Then a significant study on the load function showed expected behaviors and mechanisms regarding the viscoelastic nature of the material. This study also highlights the experimental challenges to face since rubbers are time-dependent and the importance of establishing loading-holding-unloading procedures.

Finally, indent profiles were performed using established indentation procedure. They provided a mapping of the heterogeneity of the material's mechanical response probably related to the curing gradient, at a microscopic scale. This would mean that the vulcanization of this FKM is not homogeneous.

Otherwise, the comparison with this study with literature allows to conclude that, in terms of moduli gradients, a great diversity of trends can be observed on both elastomers and polymers: there could be positive, negative or complex wavy evolutions, or even a non-variation. It is important to note that origins of these local gradients are numerous: chemical diffusions, thermal gradients or morphological due to the manufacturing process. These differences in mechanical behaviors significantly prove the relevance of using a local probe such as Instrumented Indentation to identify the presence and the type of skin-core effects.

This work opens new prospects. First, IIT could be used as a tool to appreciate the viscoelasticity of such materials and thus could open a new field study about the local behavior. Also, in terms of gradients observations applied on rubbers, it would be possible to capture local chemical diffusions as well as aging or fatigue effects.

Data Availability

The raw data required to reproduce these findings cannot be shared at this time as the data also forms part of an ongoing study.

The processed data required to reproduce these findings cannot be shared at this time as the data also forms part of an ongoing study.

References

[1] D. Tabor, The hardness of solids, Rev. Phys. Technol. 1 (1970) 145–179. doi:10.1088/0034-6683/1/3/I01.

[2] S.M. Walley, Historical origins of indentation hardness testing, Mater. Sci. Technol. 28 (2012) 1028–1044. doi:10.1179/1743284711Y.0000000127.

[3] R.A. Shanks, I. Kong, General Purpose Elastomers : Structure , Chemistry , Physics and Performance, in: Adv. Elastomers I, 2013: pp. 11–45. doi:10.1007/978-3-642-20925-3.

[4] A. Lion, On the large deformation behaviour of reinforced rubber at different temperatures, J. Mech. Phys. Solids. 45 (1997) 1805–1834.

[5] T. Riccò, A. Pegoretti, Nonlinear Dynamic Behavior of Rubber Compounds : Construction of Dynamic Moduli Generalized Master Curves, Polym. Eng. Sci. 40 (2000) 2227–2231.

[6] A.F.M.S. Amin, A. Lion, S. Sekita, Y. Okui, Nonlinear dependence of viscosity in modeling the rate-dependent response of natural and high damping rubbers in compression and shear : Experimental identification and numerical verification, Int. J. Plast. 22 (2006) 1610–1657. doi:10.1016/j.ijplas.2005.09.005.

[7] J.S. Dick, Vulcanizate Physical Properties, Performance Characteristics, and Testing, in: Rubber Technol., Second Edi, 2009: p. 567.

[8] M. Cheng, W. Chen, Experimental investigation of the stress – stretch behavior of EPDM rubber with loading rate effects, Int. J. Solids Struct. 40 (2003) 4749–4768. doi:10.1016/S0020-7683(03)00182-3.

[9] C.R. Siviour, J.L. Jordan, High Strain Rate Mechanics of Polymers : A Review, J. Dyn. Behav. Mater. 2 (2016) 15–32. doi:10.1007/s40870-016-0052-8.

[10] C.A. Gray, H. Muranko, Studies of Robustness of Industrial Aciniform Aggregates and Agglomerates — Carbon Black and Amorphous Silicas : A Review Amplified by New Data, J. Occup. Environ. Med. 48 (2006) 1279–1290. doi:10.1097/01.jom.0000251477.40643.2a.

[11] S. Araby, Q. Meng, L. Zhang, I. Zaman, P. Majewski, J. Ma, Elastomeric composites based on carbon nanomaterials, Nanotechnology. 26 (2015) 23. doi:10.1088/0957-4484/26/11/112001.

[12] Z. Rigbi, Reinforcement of Rubber by Carbon Black, Rubber Chem. Technol. 55 (1982) 1180–1220.

[13] A.R. Payne, R.E. Whittaker, Reinforcement of rubber with carbon black, Composites. 1 (1970) 203–214.

[14] A.R. Payne, R.E. Whittaker, Effect of Vulcanization on the Low-Strain Dynamic Properties of Filled Rubbers, J. Appl. Polym. Sci. 16 (1972) 1191–1212.

[15] A.E. Zaikin, R.Y. Mindubaev, V.P. Arkhireev, A study of the localization of carbon black particles at the interfaces in heterogeneous polymer blends, Colloid J. 61 (1999) 459–466.

[16] H. Hertz, On the contact of elastic solids, J. Für Die Reine Und Angew. Math. 92 (1881) 156–171.

[17] H. Hertz, On hardness, Verhandlungen Des Vereins Zur Beförderung Des Gewerbefleisses. 61 (1882) 21.

[18] M.J. Boussinesq, Application des potentiels à l'étude de l'équilibre et du mouvement des solides élastiques, principalement au calcul des déformations et des pressions que produisent, dans les solides, des efforts quelquonques exercés sur une petite partie de leur surface, Lille, 1885.

[19] A.E.H. Love, Boussinesq's problem for a rigid cone, Q. J. Math. 10 (1939) 161–175. doi:10.1093/qmath/os-10.1.161.

[20] I.N. Sneddon, The relation between load and penetration in the axisymmetric Boussinesq problem for a punch of arbitrary profile, Int. J. Eng. Sci. 3 (1965) 47–57. doi:10.1016/0020-7225(65)90019-4.

[21] W.C. Oliver, G.M. Pharr, An Improved Technique for Determining Hardness and Elastic-Modulus Using Load and Displacement Sensing Indentation Experiments, J. Mater. Res. 7 (1992) 1564–1583. doi:10.1557/.

[22] W.C. Oliver, G.M. Pharr, Measurement of hardness and elastic modulus by instrumented indentation: Advances in understanding and refinements to methodology, J. Mater. Res. 19 (2004) 3–20. doi:10.1557/jmr.2004.19.1.3.

[23] A.C. Fischer-Cripps, Nanoindentation, Third Edit, Springer New York, New York, NY, 2011. doi:10.1007/978-1-4419-9872-9.

[24] G. Constantinides, K.S. Ravi Chandran, F.-J. Ulm, K.J. Van Vliet, Grid indentation analysis of composite microstructure and mechanics: Principles and validation, Mater. Sci. Eng. A. 430 (2006) 189–202. doi:10.1016/j.msea.2006.05.125.

[25] J. Nohava, P. Hausild, N.X. Randall, G. Favaro, Grid nanoindentation on multiphase materials for mapping the mechanical properties of complex microstructures, in: IMEKO 2010 TC3, TC5 TC22 Conf. Metrol. Mod. Context, Pattaya, Chonburi, Thailand, 2010: pp. 195–198.

[26] F.J. Ulm, M. Vandamme, C. Bobko, J.A. Ortega, K. Tai, C. Ortiz, Statistical indentation techniques for hydrated nanocomposites: Concrete, bone, and shale, J. Am. Ceram. Soc. 90 (2007) 2677–2692. doi:10.1111/j.1551-2916.2007.02012.x.

[27] G. Constantinides, F.-J. Ulm, The nanogranular nature of C-S-H, J. Mech. Phys. Solids. 55 (2007) 64–90. doi:10.1016/j.jmps.2006.06.003.

[28] M.S. Bobji, S.K. Biswas, Estimation of hardness by nanoindentation of rough surfaces, J. Mater. Res. 13 (1998) 3227–3233. doi:10.1557/JMR.1998.0438.

[29] H. Kesari, J.C. Doll, B.L. Pruitt, W. Cai, A.J. Lew, Role of surface roughness in hysteresis during adhesive elastic contact, Philos. Mag. Lett. 90 (2010) 891–902.

doi:10.1080/09500839.2010.521204.

[30] J.-Y. Kim, S.-K. Kang, J.-J. Lee, J. Jang, Y.-H. Lee, D. Kwon, Influence of surface-roughness on indentation size effect, Acta Mater. 55 (2007) 3555–3562. doi:10.1016/j.actamat.2007.02.006.

[31] L. Chen, A. Ahadi, J. Zhou, J.-E. Ståhl, Modeling effect of surface roughness on nanoindentation tests, Procedia CIRP. 8 (2013) 334–339. doi:10.1016/j.procir.2013.06.112.

[32] J. Němeček, L. Zhang, T. Ohmura, K. Tsuzaki, B.A. Latella, M. V. Swain, M. Ignat, Nanoindentation in Materials Science, Second Edi, InTech, 2012. doi:10.5772/2829.

[33] K.T. Gillen, E.R. Terrill, R.M. Winter, Modulus Mapping of Rubbers Using Micro- and Nano-Indentation Techniques, Rubber Chem. Technol. 74 (2001) 428–450. doi:10.5254/1.3547646.

[34] P. Pourmand, E. Linde, M.S. Hedenqvist, I. Furó, S.V. Dvinskikh, U.W. Gedde, Profiling of thermally aged EPDM seals using portable NMR, indenter measurements and IR spectroscopy facilitating separation of different deterioration mechanisms, Polym. Test. 53 (2016) 77–84.

[35] A. Kömmling, M. Jaunich, P. Pourmand, D. Wolff, U.W. Gedde, Influence of Ageing on Sealability of Elastomeric O-Rings, Macromol. Symp. 373 (2017) 1600157. doi:https://doi.org/10.1002/masy.201600157.

[36] F. Carrillo, S. Gupta, M. Balooch, S.J. Marshall, G.W. Marshall, L. Pruitt, C.M. Puttlitz, Nanoindentation of polydimethylsiloxane elastomers: Effect of crosslinking, work of adhesion, and fluid environment on elastic modulus, J. Mater. Res. 20 (2005) 2820–2830. doi:10.1557/JMR.2005.0354.

[37] Y.Y. Lim, M.M. Chaudhri, Indentation of rigid cones into conical holes molded in elastic blocks, J. Appl. Phys. 98 (2005) 73518. doi:10.1063/1.2060933.

[38] C.A. Charitidis, Nanoscale Deformation and Nanomechanical Properties of Polydimethylsiloxane (PDMS), Ind. Eng. Chem. Res. 50 (2011) 565–570. doi:10.1021/ie100099g.

[39] F. Alisafaei, C.-S. Han, S.H. Reza Sanei, On the time and indentation depth dependence of hardness, dissipation and stiffness in polydimethylsiloxane, Polym. Test. 32 (2013) 1220–1228. doi:10.1016/j.polymertesting.2013.07.013.

[40] J.C. Kohn, D.M. Ebenstein, Eliminating adhesion errors in nanoindentation of compliant polymers and hydrogels, J. Mech. Behav. Biomed. Mater. 20 (2013) 316–326. doi:10.1016/j.jmbbm.2013.02.002.

[41] A.J. Wrucke, C.-S. Han, P. Majumdar, Indentation size effect of multiple orders of magnitude in polydimethylsiloxane, J. Appl. Polym. Sci. 128 (2013) 258–264. doi:10.1002/app.38161.

[42] D. Berthier, M.-P. Deffarges, N. Berton, M. Venin, F. Lacroix, B. Schmaltz, Y. Tendron, E. Pestel, POSS Nanofiller-Induced Enhancement of the Thermomechanical Properties in a Fluoroelastomer, Materials (Basel). 11 (2018) 1358. doi:10.3390/ma11081358.

[43] K. Fu, Y. Chang, Y. Tang, B. Zheng, Effect of loading rate on the creep behaviour of epoxy resin insulators by nanoindentation, J. Mater. Sci. Mater. Electron. 25 (2014) 3552–3558. doi:10.1007/s10854-014-2055-3.

[44] C.C. Huang, M.K. Wei, S. Lee, Transient and steady-state nanoindentation creep of polymeric materials, Int. J. Plast. 27 (2011) 1093–1102. doi:10.1016/j.ijplas.2010.11.005.

[45] T. Jin, X. Niu, G. Xiao, Z. Wang, Z. Zhou, G. Yuan, X. Shu, Effects of experimental variables on PMMA nano-indentation measurements, Polym. Test. 41 (2015) 1–6. doi:10.1016/j.polymertesting.2014.09.015.

[46] M. Hardiman, T.J. Vaughan, C.T. McCarthy, The effects of pile-up, viscoelasticity and hydrostatic stress on polymer matrix nanoindentation, Polym. Test. 52 (2016) 157–166. doi:https://doi.org/10.1016/j.polymertesting.2016.04.003.

[47] A.H.W. Ngan, B. Tang, Viscoelastic effects during unloading in depth-sensing indentation, J. Mater. Res. 17 (2002) 2604–2610. doi:10.1557/JMR.2002.0377.

[48] A.H. Tsou, A.D. Westwood, J.S. Schulze, E.G. Herbert, Cure state distributions in rubbers by dynamic nano-indentation, Rubber Chem. Technol. 77 (2004) 678–690. doi:10.5254/1.3547844.

[49] D.M. Bielinski, Surface Properties of Polymers and Rubber Measured by Nanoindentation, in: Mater. Charact., 2015: pp. 91–115. doi:10.4032/9789814613071.

[50] E. Le Bourhis, G. Patriarche, Nanoindentation response of a single micrometer-sized GaAs wall, Appl. Phys. Lett. 86 (2005) 1–3. doi:10.1063/1.1904711.

[51] E. Le Bourhis, G. Patriarche, Mechanical response of wall-patterned GaAs surface, Acta Mater. 53 (2005) 1907–1912. doi:10.1016/j.actamat.2005.01.001.

[52] J. Persson, J.M. Zhou, J.E.- Ståhl, Characterizing the mechanical properties of skin-core structure in polymer molding process by nanoindentation, in: Swedish Prod. Symp., 2014: p. 9.

[53] J. Chu, Characterization of the Micro Injection Molding Process and Its Products, McGill University, Montreal, Quebec, Canada, 2009.

Figure Captions

Figure 1: Surface relief vs. typical contact dimension of an indent made at 1 mN, a) on the rough molded surface and b) on the smooth, razor-blade-prepared surface of FKM elastomer

Figure 2: Reproducibility of the indentation hystereses for two FKM elastomer surfaces, a) on the rough molded surface and b) on the smooth, razor-blade-prepared surface (set-up : maximal force of 1 mN, loading rate 0.01 mN/s, holding time 300 s and unloading rate 0.01 mN/s)

Figure 3: T.E.M. observation of the FKM elastomer microstructure vs. typical projected contact dimension of an indent made under 1 mN

Figure 4: Loading curves in FKM elastomer prepared with razor blade with different loading rates in the range 0.001 to 0.5 mN/s

Figure 5: Loading, holding and maximal displacements (h_L, h_H and h_{max} respectively) in FKM elastomer prepared with razor blade as a function of the loading rate

Figure 1

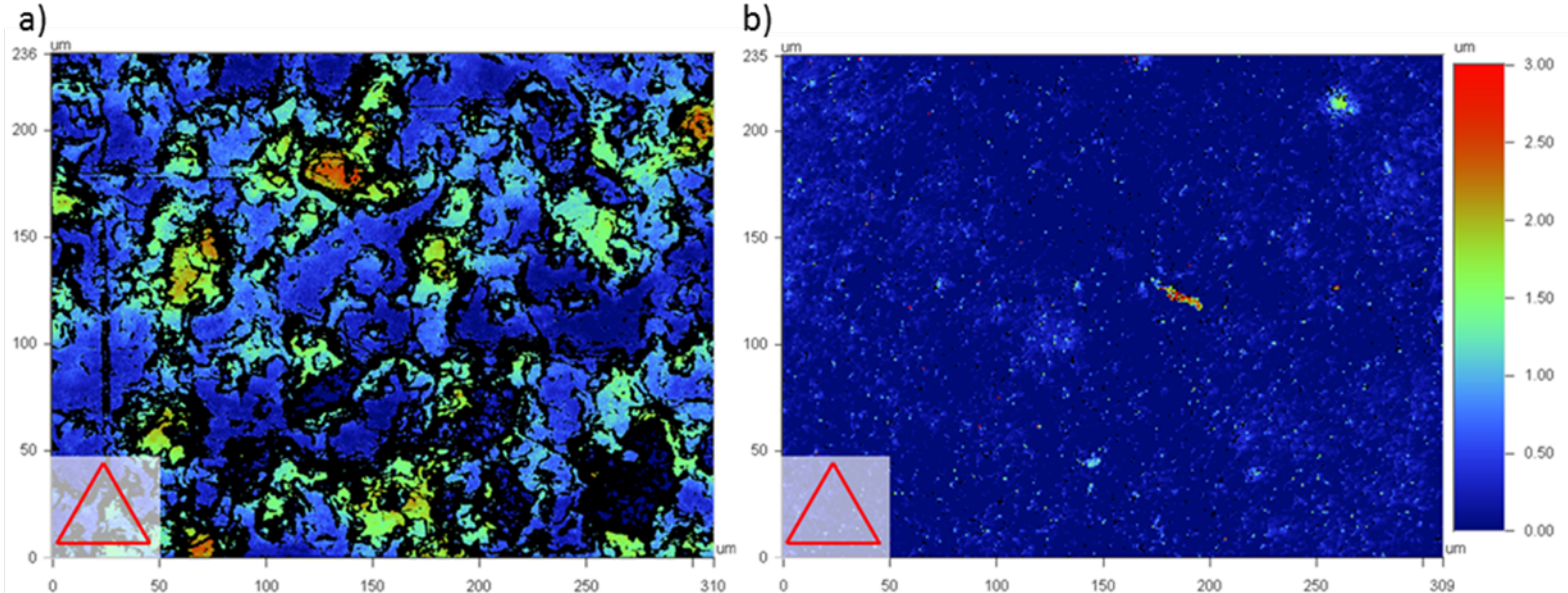
a)
b)
um
236
200
150
100
50
0
0
50
100
150
200
250
310
um
235
200
150
100
50
0
0
50
100
150
200
250
309
um
3.00
2.50
2.00
1.50
1.00
0.50
0.00

FIG 2

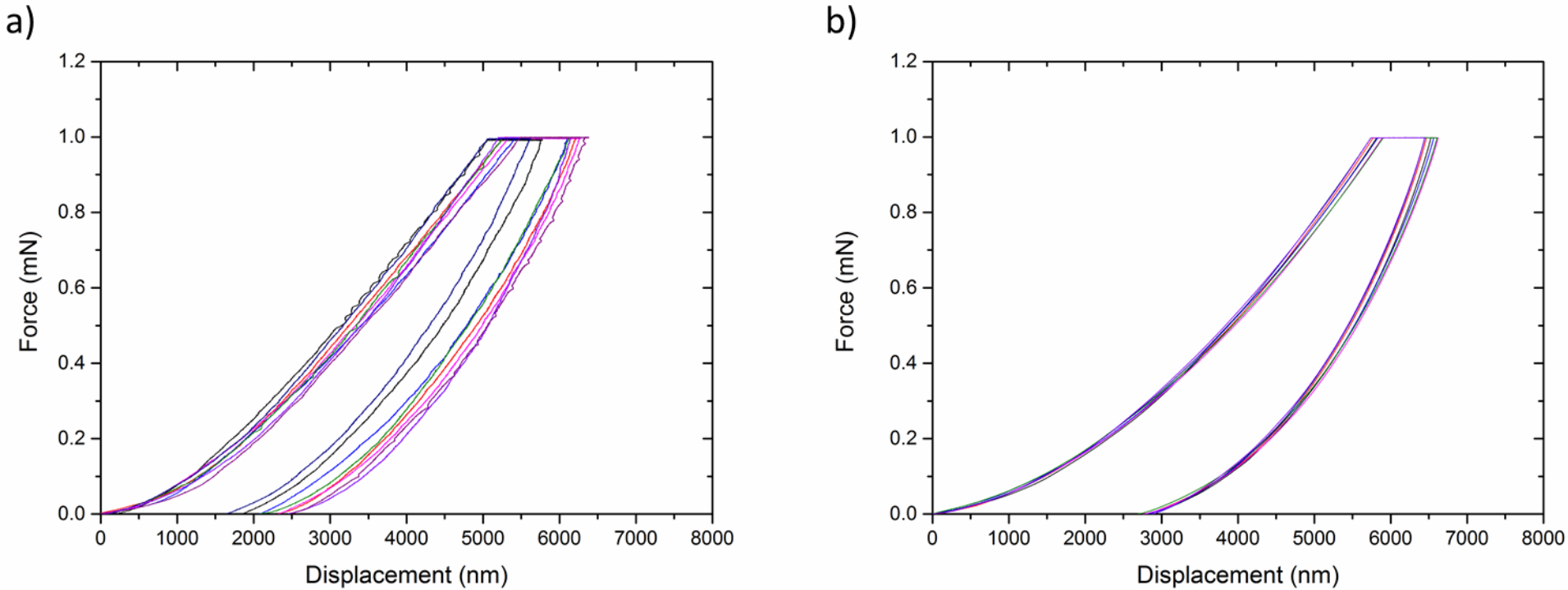
a)
b)
Force (mN)
Displacement (nm)
0.0
0.2
0.4
0.6
0.8
1.0
1.2
0
1000
2000
3000
4000
5000
6000
7000
8000

Figure 3

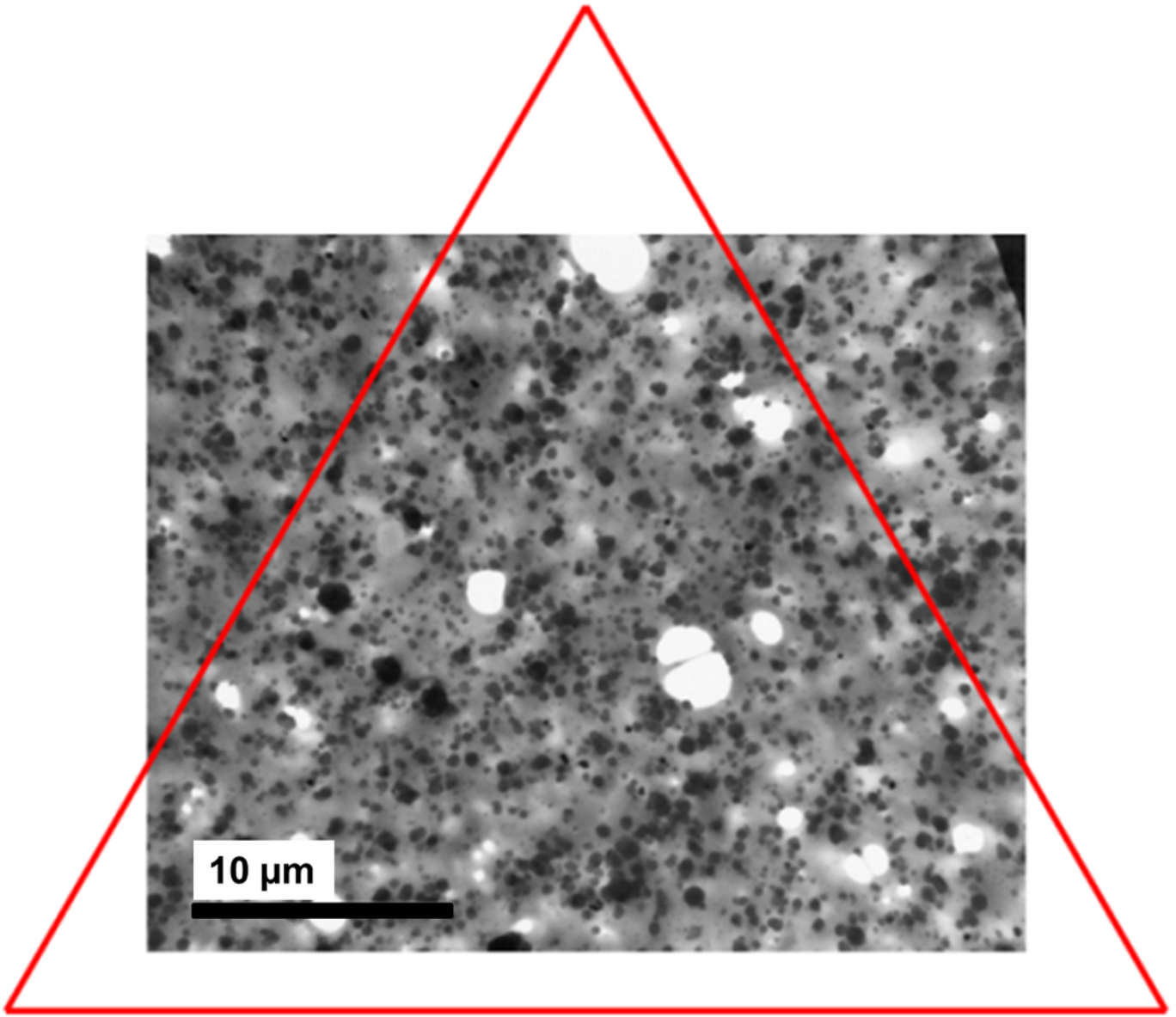

FIG 4

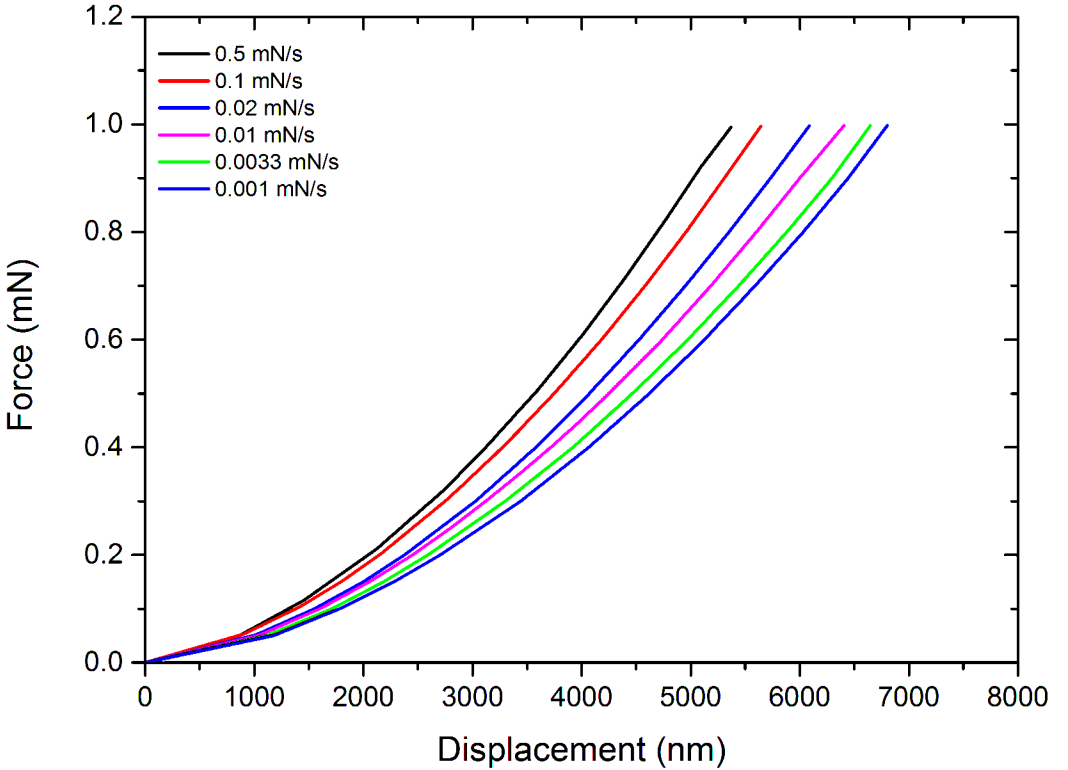
0.5 mN/s
0.1 mN/s
0.02 mN/s
0.01 mN/s
0.0033 mN/s
0.001 mN/s
Force (mN)
Displacement (nm)
0.0
0.2
0.4
0.6
0.8
1.0
1.2
0
1000
2000
3000
4000
5000
6000
7000
8000

FIG 5

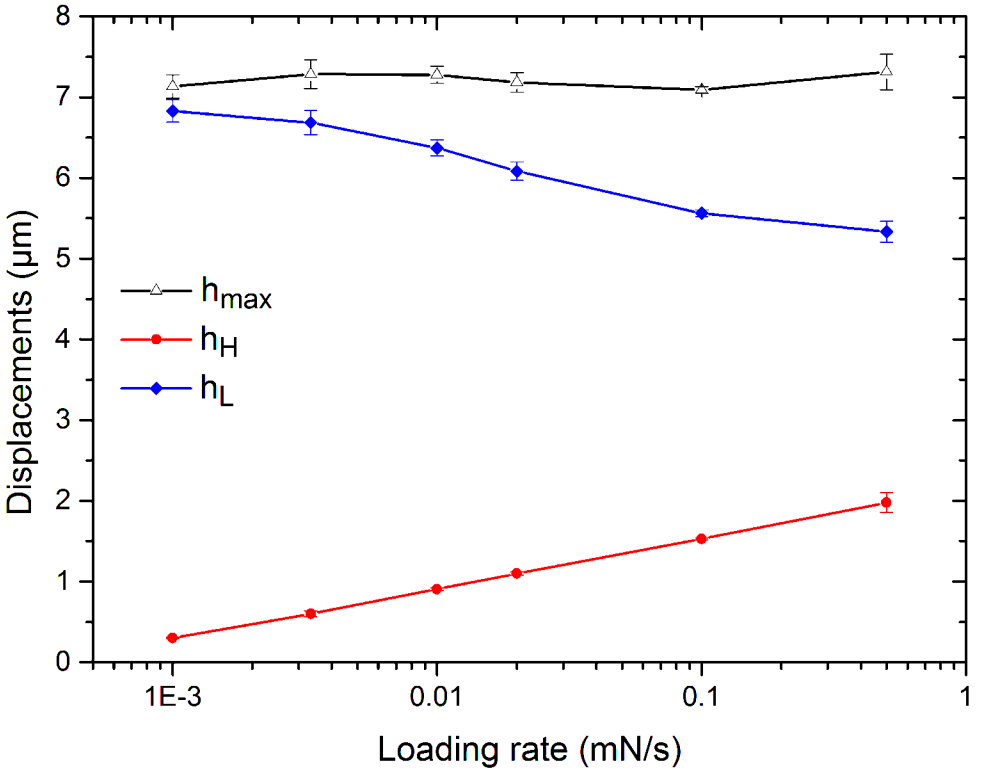
Displacements (μm)
Loading rate (mN/s)
1E-3
0.01
0.1
1
0
1
2
3
4
5
6
7
8
h_{max}
h_H
h_L

FIG 6

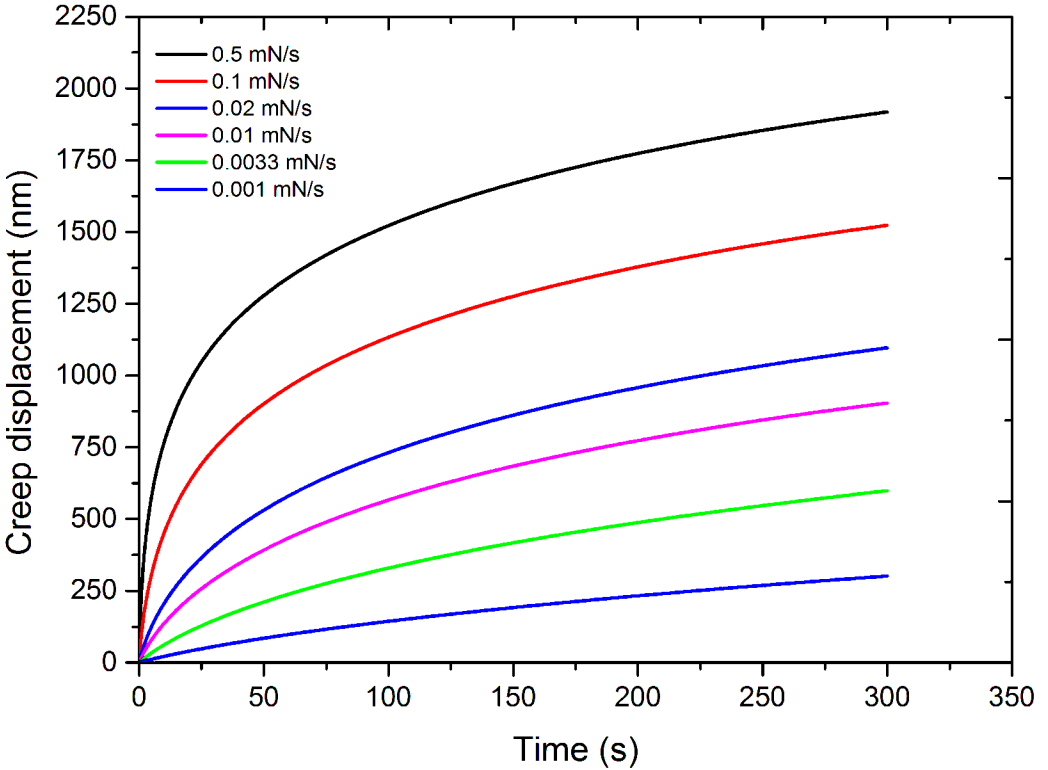
0.5 mN/s
0.1 mN/s
0.02 mN/s
0.01 mN/s
0.0033 mN/s
0.001 mN/s
Creep displacement (nm)
Time (s)
0
250
500
750
1000
1250
1500
1750
2000
2250
0
50
100
150
200
250
300
350

FIG 7

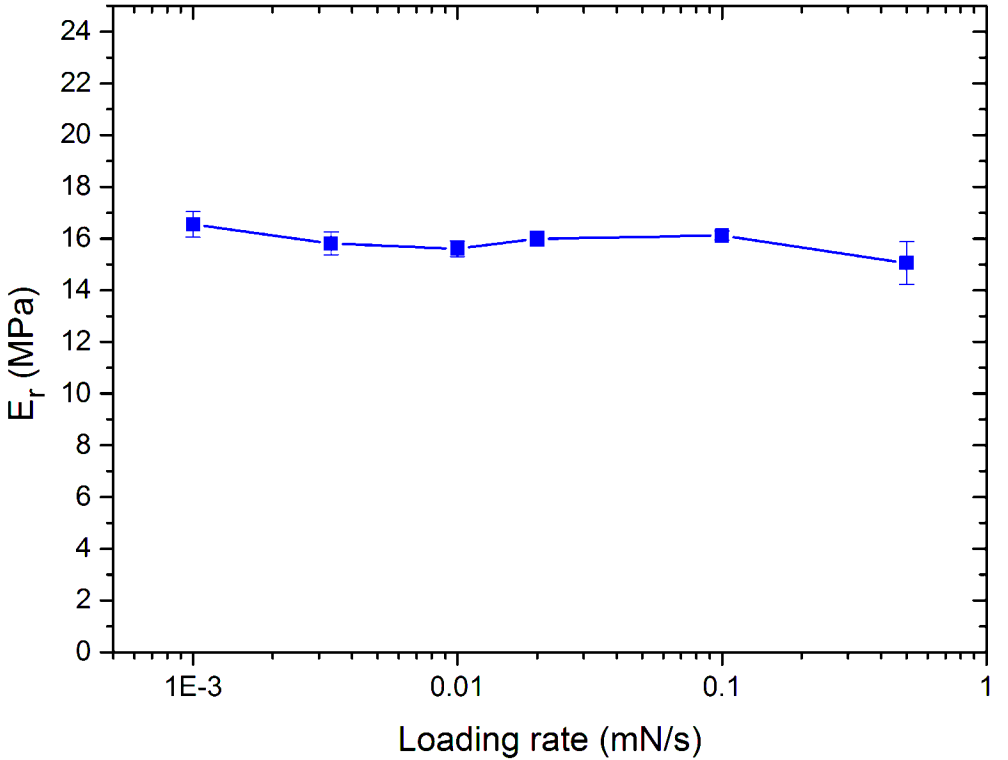

FIG 8

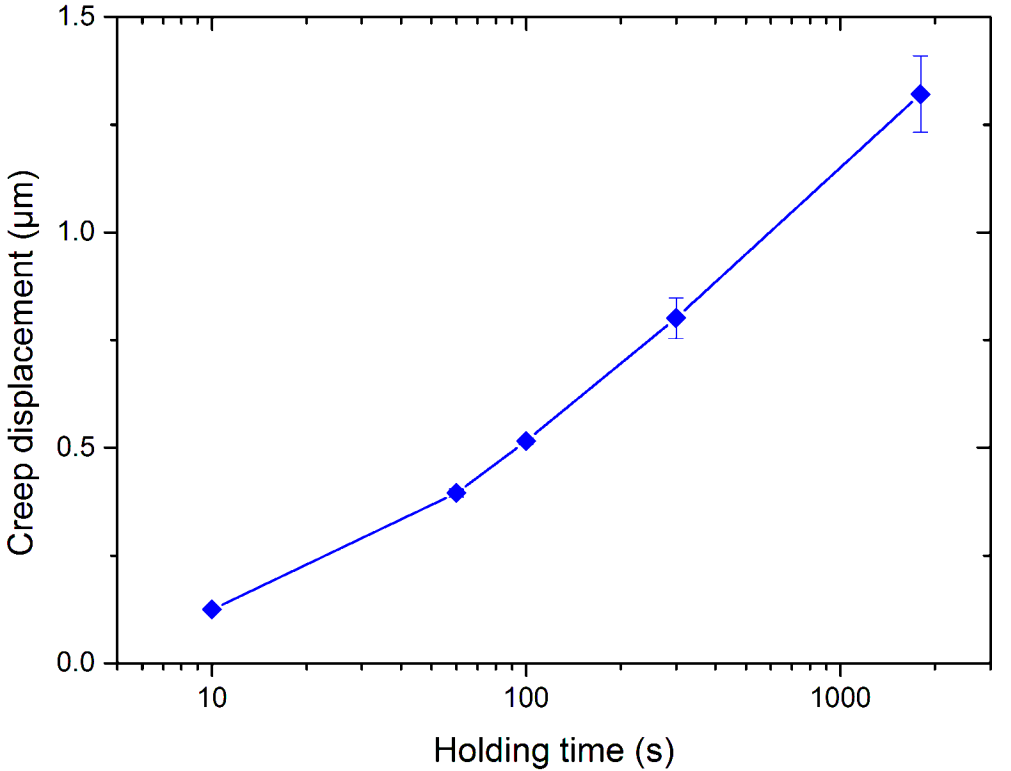

FIG 9

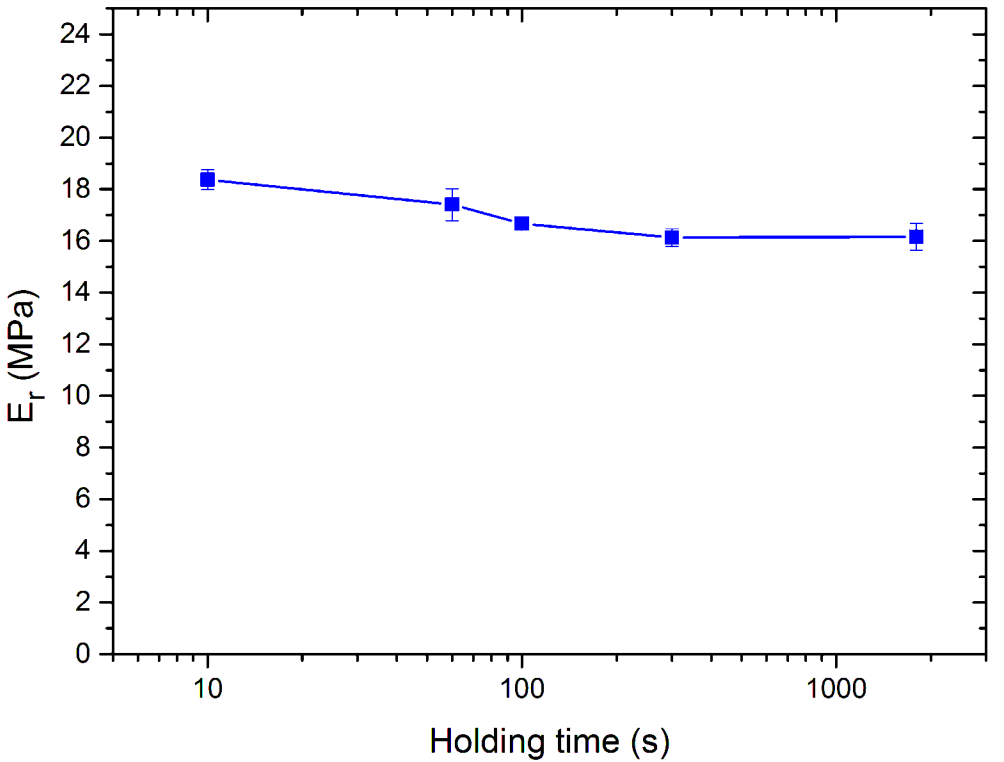

FIG 10

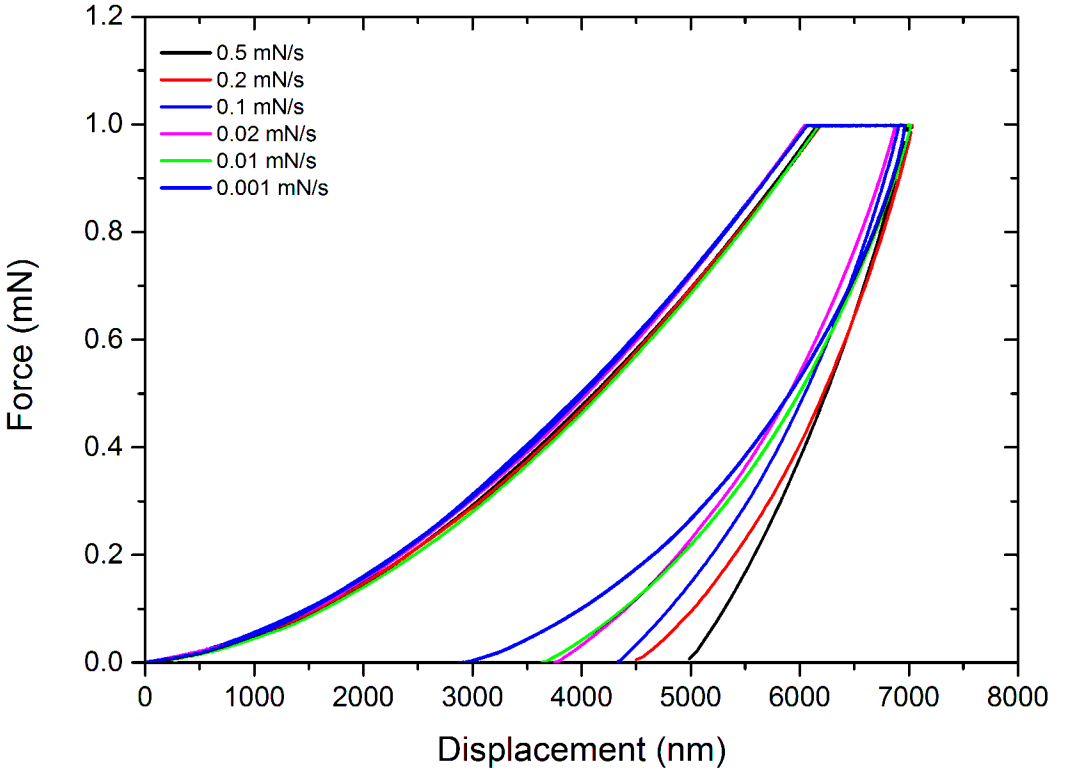
0.5 mN/s
0.2 mN/s
0.1 mN/s
0.02 mN/s
0.01 mN/s
0.001 mN/s
Force (mN)
Displacement (nm)
0.0
0.2
0.4
0.6
0.8
1.0
1.2
0
1000
2000
3000
4000
5000
6000
7000
8000

FIG 11

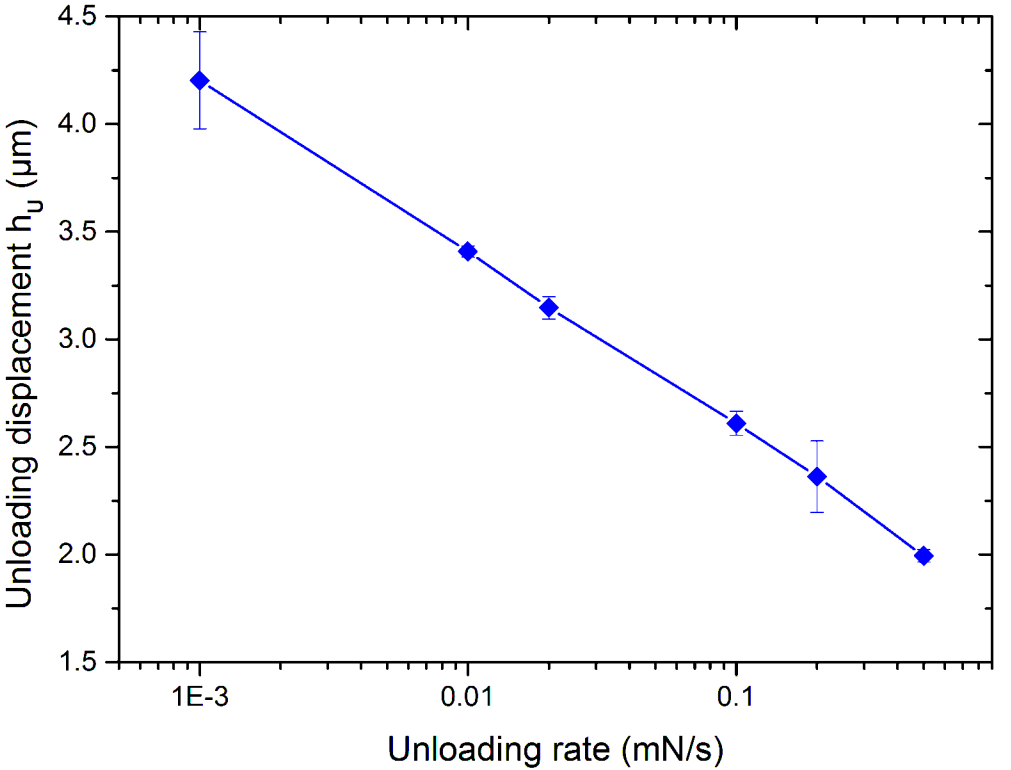
4.5
4.0
3.5
3.0
2.5
2.0
1.5
Unloading displacement h_u (μm)
1E-3
0.01
0.1
Unloading rate (mN/s)

FIG 12

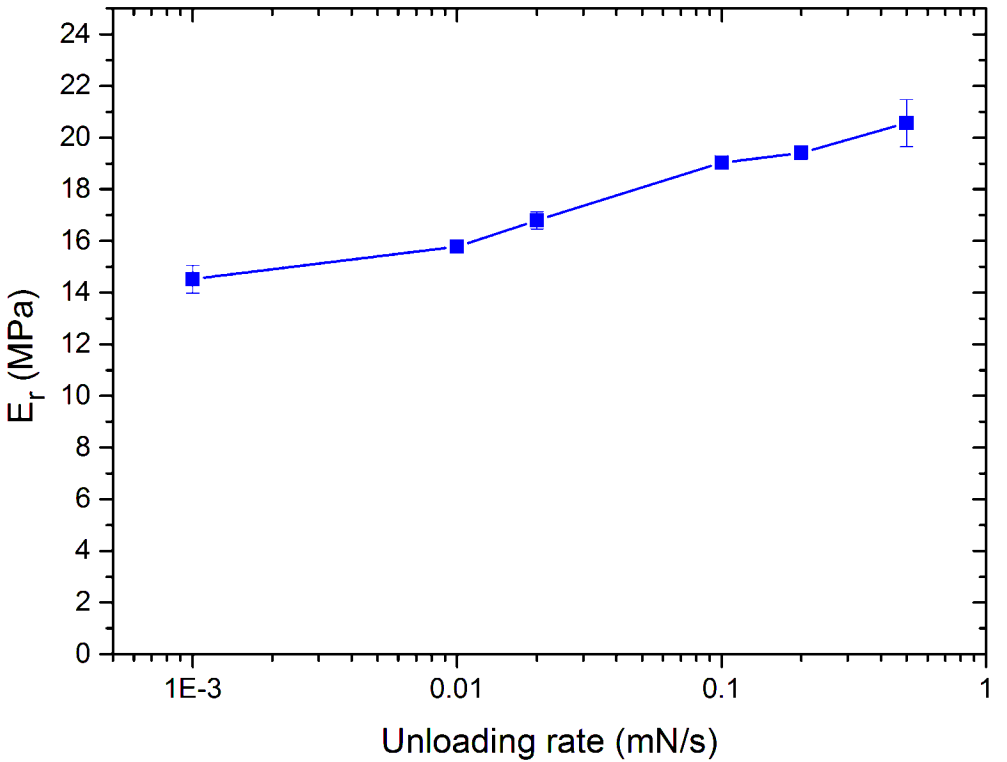
24
22
20
18
16
14
12
10
8
6
4
2
0
E_r (MPa)
1E-3
0.01
0.1
1
Unloading rate (mN/s)

FIG 13

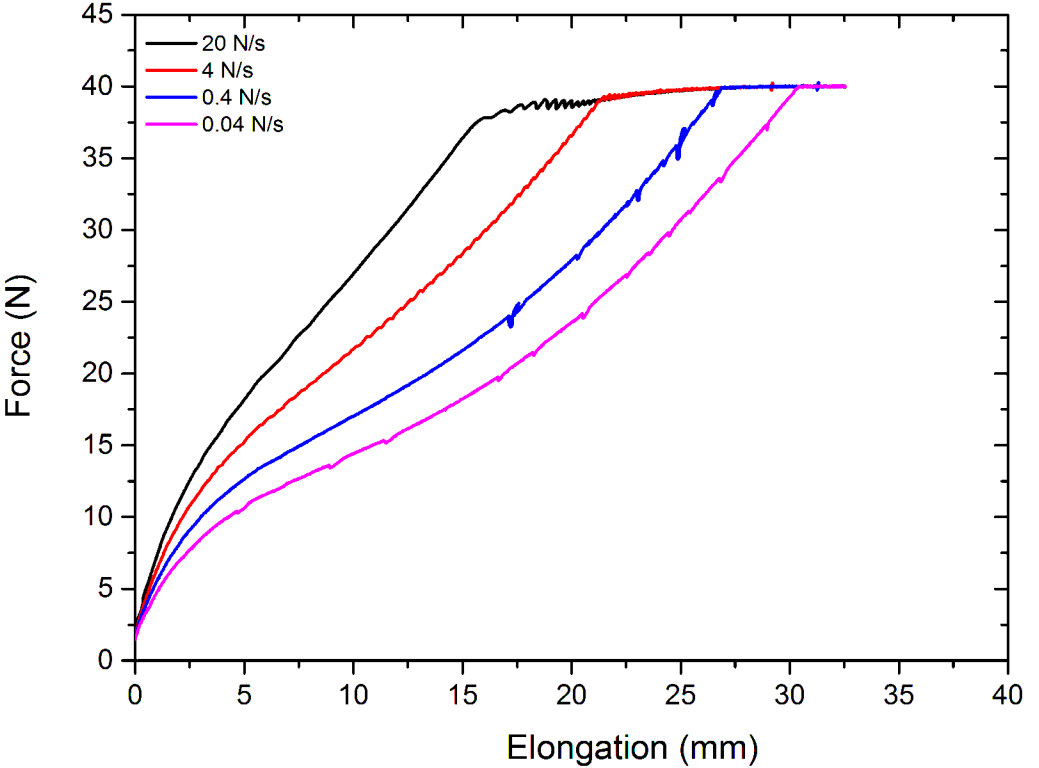
20 N/s
4 N/s
0.4 N/s
0.04 N/s
Force (N)
Elongation (mm)
0
5
10
15
20
25
30
35
40
45

FIG 14

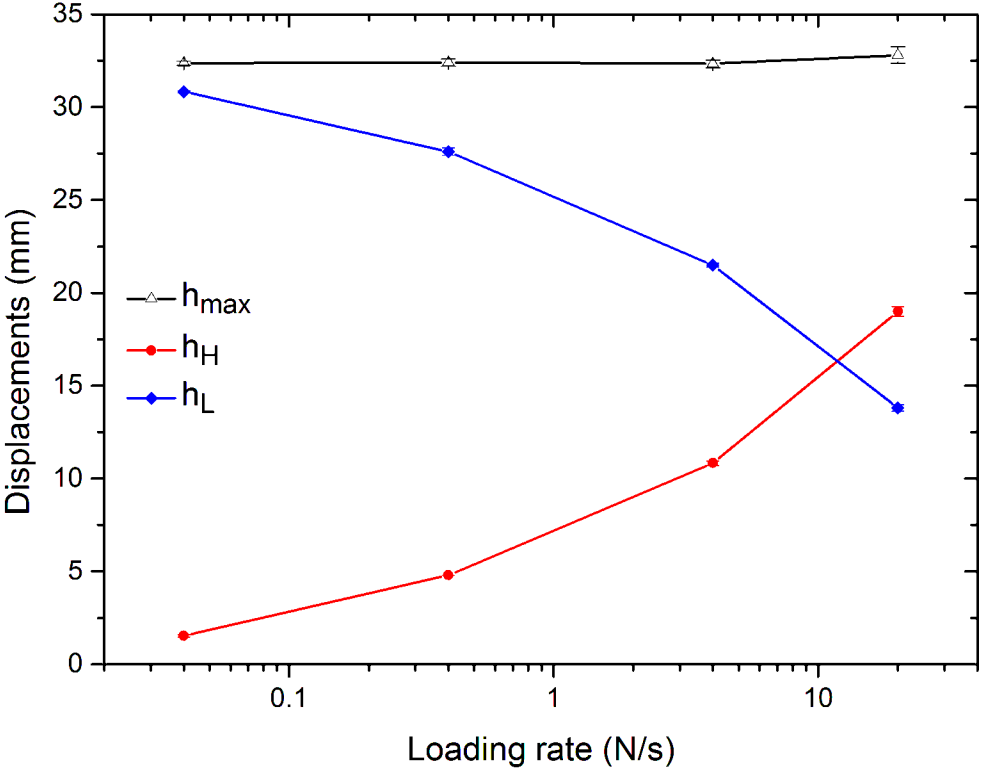
35
30
25
20
15
10
5
0
Displacements (mm)
h_max
h_H
h_L
0.1
1
10
Loading rate (N/s)

FIG 15

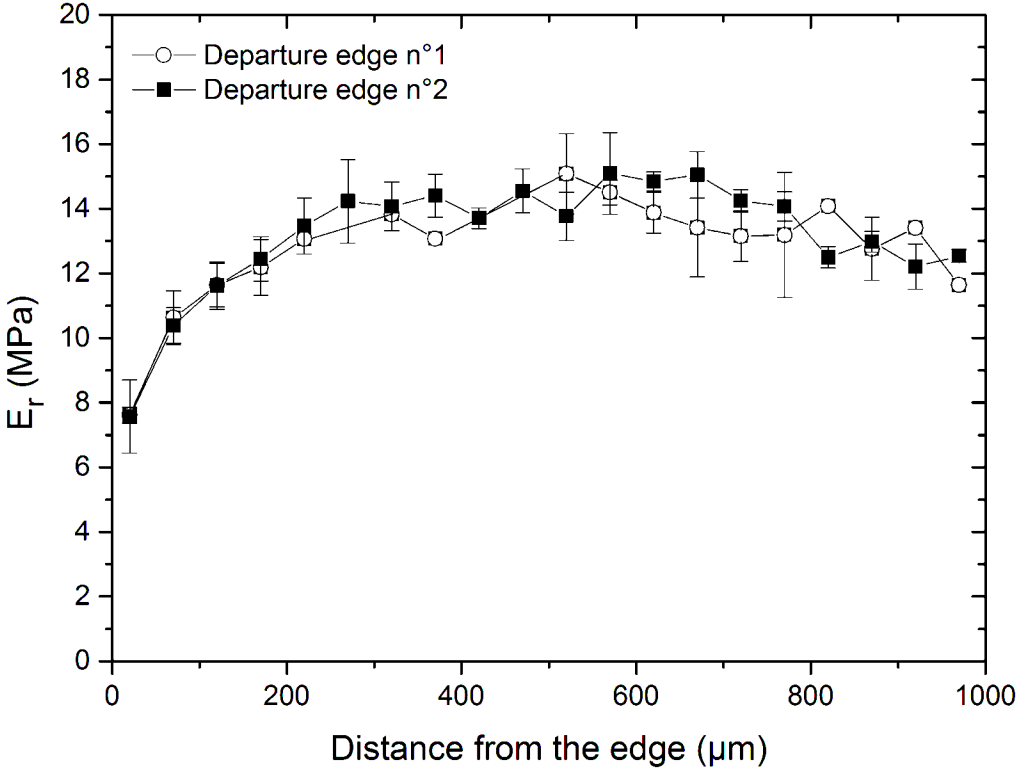
Departure edge n°1
Departure edge n°2
E_r (MPa)
Distance from the edge (µm)
0
2
4
6
8
10
12
14
16
18
20
0
200
400
600
800
1000

FIG 16

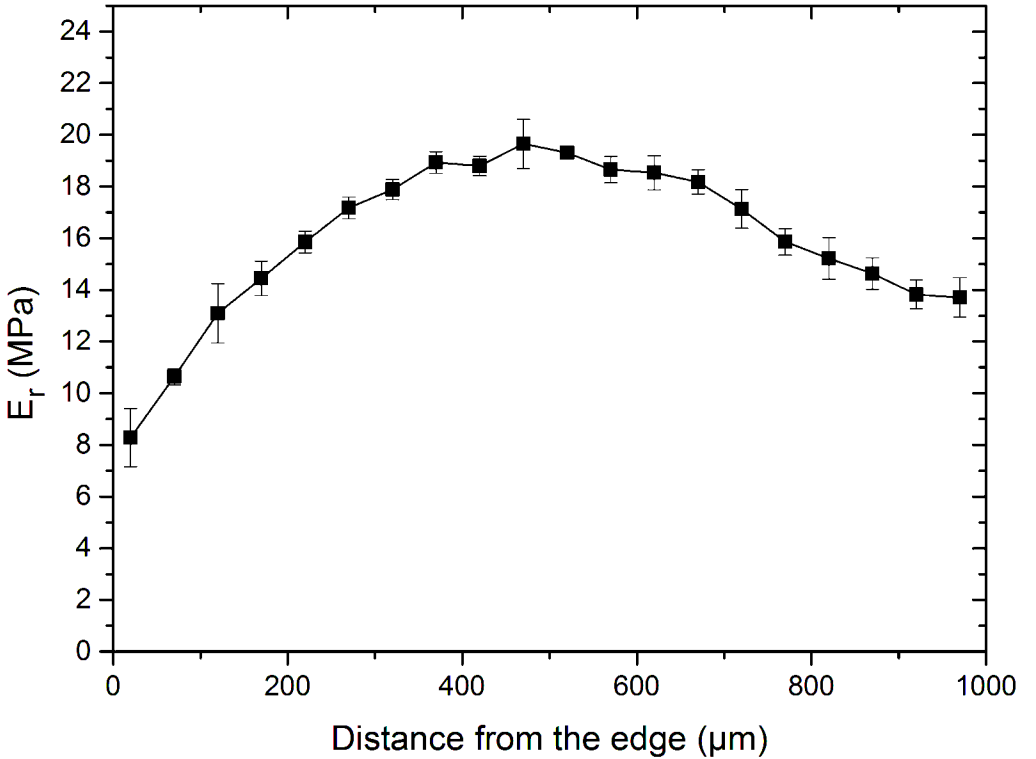
24
22
20
18
16
14
12
10
8
6
4
2
0
E_r (MPa)
0
200
400
600
800
1000
Distance from the edge (μm)

FIG 17

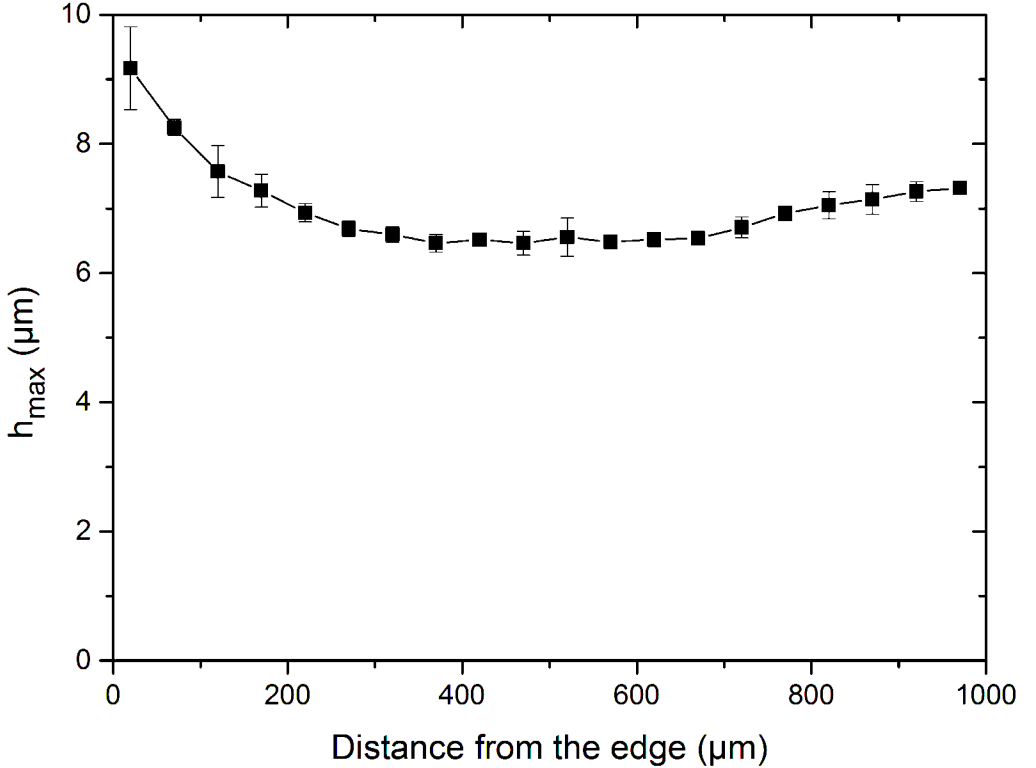
10
8
6
4
2
0
h_{max} (µm)
0
200
400
600
800
1000
Distance from the edge (µm)